ORIGINAL RESEARCH

Open Access

CrossMark

Quantification of myocardial blood flow with ^{82}Rb: Validation with ^{15}O-water using time-of-flight and point-spread-function modeling

Mary Germino[1,4]* ⬤, Jim Ropchan[2], Tim Mulnix[2], Kathryn Fontaine[2], Nabeel Nabulsi[2], Eric Ackah[3], Herman Feringa[3], Albert J. Sinusas[3], Chi Liu[1,2] and Richard E. Carson[1,2]

Abstract

Background: We quantified myocardial blood flow with ^{82}Rb PET using parameters of the generalized Renkin-Crone model estimated from ^{82}Rb and ^{15}O-water images reconstructed with time-of-flight and point spread function modeling. Previous estimates of rubidium extraction have used older-generation scanners without time-of-flight or point spread function modeling. We validated image-derived input functions with continuously collected arterial samples.

Methods: Nine healthy subjects were scanned at rest and under pharmacological stress on the Siemens Biograph mCT with ^{82}Rb and ^{15}O-water PET, undergoing arterial blood sampling with each scan. Image-derived input functions were estimated from the left ventricle cavity and corrected with tracer-specific population-based scale factors determined from arterial data. Kinetic parametric images were generated from the dynamic PET images by fitting the one-tissue compartment model to each voxel's time activity curve. Mean myocardial blood flow was determined from each subject's ^{15}O-water k_2 images. The parameters of the generalized Renkin-Crone model were estimated from these water-based flows and mean myocardial ^{82}Rb K_1 estimates.

Results: Image-derived input functions showed improved agreement with arterial measurements after a scale correction. The Renkin-Crone model fit ($a = 0.77$, $b = 0.39$) was similar to those previously published, though b was lower.

Conclusions: We have presented parameter estimates for the generalized Renkin-Crone model of extraction for ^{82}Rb PET using human ^{82}Rb and ^{15}O-water PET from high-resolution images using a state-of-the-art time-of-flight-capable scanner. These results provide a state-of-the-art methodology for myocardial blood flow measurement with ^{82}Rb PET.

Keywords: Myocardial blood flow, Rubidium-82 PET, Image-derived input function, TOF PET

Background

Cardiac perfusion PET with ^{82}Rb is clinically useful for diagnosing coronary artery disease [1–4]. Quantification of myocardial blood flow (MBF) and coronary flow reserve (CFR) can be obtained from ^{82}Rb PET but relies on accurately modeling the extraction fraction of rubidium by myocardial tissue, which is nonlinearly related to

flow as described by the generalized Renkin-Crone model [5–8]. Uncertainty in the extraction model parameters causes much of the uncertainty in MBF [9].

Several groups have reported generalized Renkin-Crone model parameters for rubidium using canine or human MBF data from microspheres [10], ^{13}N-ammonia [5, 11], and ^{15}O-water [12, 13]. Most of these studies used older-generation PET systems with 2D or reduced-dose 3D acquisitions. To our knowledge, no extraction fraction estimations have been made using scanners with time-of-flight (TOF) capabilities; for ^{82}Rb PET, such systems provide better signal-to-noise ratios than non-

* Correspondence: mary.germino@yale.edu
[1]Biomedical Engineering, Yale University, New Haven, CT, USA
[4]PET Center, Yale School of Medicine, PO Box 208048, New Haven, CT 06520-8048, USA
Full list of author information is available at the end of the article

Germino et al. EJNMMI Research (2016) 6:68

Page 2 of 12

TOF systems [14, 15] and parametric images with lower standard error. Further, when point spread function (PSF) modeling is included in reconstruction, MBF estimates from ^{82}Rb PET may be higher [16]; however, such calculations were performed using an extraction model [11] derived from non-TOF, non-PSF images. Presotto et al. [17] demonstrated the quantitative superiority of PSF + TOF for dynamic cardiac reconstructions using a thorax/heart phantom filled with either ^{18}F alone or ^{18}F and ^{13}N (to simulate dynamically varying contrast), in both static and moving configurations.

Errors in the input function, another critical component of kinetic modeling, can substantially bias kinetic parameter estimates [18]. For practical reasons, image-derived input functions (IDIFs) are widely used in cardiac PET. IDIFs estimated from blood pool regions of cardiac images have been validated against the gold standard of arterial samples in dogs [5, 19] but not recently in humans with ^{82}Rb PET.

A recent study of five extraction model fits and three IDIF estimation methods demonstrated that these choices substantially influence MBF estimates [20]. In this work, we reexamined extraction fraction estimation in humans with paired rest and stress studies with ^{82}Rb and ^{15}O-water acquired on a state-of-the-art system, the Siemens Biograph mCT, and reconstructed images with TOF and PSF modeling. We augmented this high-quality image data with continuously sampled arterial measurements for input function validation. From these data, we provided new parameter estimates of the generalized Renkin-Crone model for rubidium extraction.

Methods
Subjects
Nine healthy subjects (five male) with no known cardiac abnormalities were studied. This study was approved by the Yale University Human Investigation Committee; all subjects signed an informed consent form. The average age was 28.4 ± 6.2 years, and average BMI was 24.7 ± 3.9 kg/m^2. Subjects abstained from caffeine for 12 h pre-imaging, and from food for 4–6 h. Before scanning, an intravenous line for tracer administration and an arterial line for blood sampling were placed.

Data acquisition
PET scans were acquired on the Biograph mCT 1104 (Siemens Healthcare, Knoxville, TN) at rest and under pharmacological stress with ^{82}Rb and ^{15}O-water for each subject. For seven subjects, the scan sequence was: ^{82}Rb rest; ^{15}O-water rest; ^{15}O-water stress; and ^{82}Rb stress. For the remaining subjects, the ^{82}Rb stress acquisition was performed directly after the ^{82}Rb rest acquisition. A 1-h interval separated each stress scan from the following acquisition, with confirmation that heart rate and

blood pressure had returned to baseline. Low-dose CT attenuation correction scans were acquired before each rest scan and after each stress scan. Pharmacological stress was induced with 0.4 mg of regadenoson, injected over 30 s, 1 min before tracer injection. The ^{82}Rb injections were performed with the CardioGen-82 (Bracco Diagnostics, Princeton, NJ) system with an infusion rate of 50 mL/min, duration of 18 ± 4 s, and mean $\pm$ SD dose of 663 ± 82 MBq. ^{15}O-water infusions with mean dose 690 ± 136 MBq were delivered over 20 s. Dosing was independent of body weight.

Arterial blood sampling and data analysis
Arterial blood was drawn from the radial artery for 7 min per scan at 4 mL per minute for seven of nine subjects and radioactivity measured with a cross-calibrated radioactivity monitor (PBS-101, Veenstra Instruments, Joure, The Netherlands). One subject chose not to have the arterial line. In another subject, the arterial line was not successfully placed. Because IDIFs were corrected with population-based scale factors, these subjects' image data were not excluded. Because the 1.25-mL infusion line for ^{82}Rb was not flushed, residual activity remained at end-of-elution. This unshielded activity contributed to the background signal detected by the radioactivity monitor, visible in the initial portion of the ^{82}Rb arterial readings before the input function peak (when measurements should be 0). To model this background signal, a decaying exponential with the ^{82}Rb decay constant was fit to the raw count data for each acquisition, between end-of-elution and the rise of the input function peak. This fitted curve was subtracted from the arterial measurements (see Additional file 1, page 1). Apart from removal of the background signal, ^{82}Rb and ^{15}O-water data were processed analogously. Corrections were applied for sensitivity, decay, and external dispersion. Sensitivity was measured by cross-calibration with phantom measurements per isotope. To correct for time delay between the left ventricle (LV) and the arterial sampling site, each acquisition's time shift was estimated by maximizing the correlation between the corrected arterial samples and the LV time activity curve (TAC).

Image reconstruction
For each injection, list-mode data were acquired for 4 min post-injection and reconstructed into 32 frames (20x3s,6x10s,6x20s) with mCT software using TOF and PSF modeling, and, for ^{82}Rb, prompt-gamma correction (OSEM with 2 iterations of 21 subsets, voxel size 2.036x2.036x2.0 mm^3). Images were post-smoothed with a 3 mm-FWHM Gaussian kernel. Summed dynamic PET images were inspected for alignment with the

Germino *et al. EJNMMI Research* (2016) 6:68

Page 3 of 12

corresponding attenuation correction CT images, and manually realigned and re-reconstructed as necessary. Images were transformed to short-axis orientation.

Kinetic modeling

The one-tissue compartment model

$$C_{\mathrm{T}}(t) = K_1 e^{-k_2 t} \otimes C_{\mathrm{A}}(t) \tag{1}$$

was used to describe the kinetics in the myocardium tissue, where K_1 is the myocardial influx rate constant, k_2 is the efflux rate constant, and $C_{\mathrm{T}}(t)$ is the tissue TAC [11, 21, 22]. Tissue TACs were converted from Bq/mL to Bq/g with an assumed tissue density of 1.05 g/mL. The arterial input function $C_{\mathrm{A}}(t)$ was estimated from either the arterial samples or the images (described below).
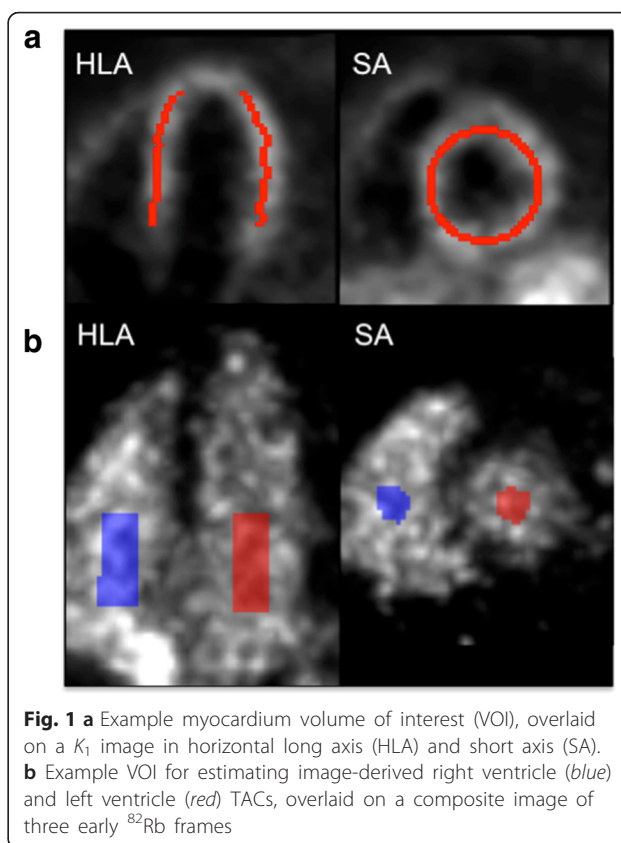
Partial volume, motion effects, and arterial blood volume were accounted for with one or two additional parameters: V_{A}, for the LV cavity spillover and arterial blood volume, and, optionally, V_{RV}, for the right ventricle (RV) cavity spillover:

$$C_{\mathrm{PET,myo}}(t) = (1 - V_{\mathrm{A}} - V_{\mathrm{RV}})C_{\mathrm{T}}(t) + V_{\mathrm{A}}C_{\mathrm{A}}(t) + V_{\mathrm{RV}}C_{\mathrm{RV}}(t) \tag{2}$$

Equation 2 was fit to each voxel TAC using the basis function method [23] and a weighted least squares (WLS) criterion, with weights based on noise equivalent counts. ^{15}O-water K_1 images were registered to the corresponding ^{82}Rb K_1 images for each subject/condition using rigid 3D versor transforms optimized by the Mattes mutual information metric. The k_2, V_{A}, and V_{RV} images were realigned using the same transforms. Left ventricular myocardium volumes-of-interest (VOIs) with approximate thickness of 4 mm were automatically determined for each subject's rest and stress scans from K_1 images, using in-house software (Fig. 1a). Model fits were performed both as three-parameter (without V_{RV}) and four-parameter fits.

Input function estimation

IDIFs were estimated from fixed-volume (6.5 mL) cylindrical VOIs manually placed towards the base of the LV and atrium blood pools of each image (Fig. 1b). The resulting TACs were compared to the measured arterial input functions (AIFs) with regard to peak concentration, tail concentration, and area under the curve (AUC). For comparisons, AIFs were resampled to the image times by averaging values within each frame. Peaks were computed as the maximal activity of each TAC. Tail activity was computed as the average concentration over 1 min starting at 2 min, 40 s post-injection. Percent difference in each metric was computed for corresponding pairs of IDIFs and AIFs and averaged across subjects.

Fig. 1 a Example myocardium volume of interest (VOI), overlaid on a K_1 image in horizontal long axis (HLA) and short axis (SA). **b** Example VOI for estimating image-derived right ventricle (*blue*) and left ventricle (*red*) TACs, overlaid on a composite image of three early ^{82}Rb frames

With a sufficiently small LV VOI, activity is often assumed to be fully recovered [10–12]; alternatively, IDIFs are sometimes corrected for partial-volume effects. For instance, [13] assumed the LV cavity TAC is a partial-volume mixture of 85 % arterial blood and 15 % myocardial tissue. We investigated partial-volume correction (PVC) methods using the AIF as the gold standard.

To assess IDIF PVC, the "true" tissue TAC C_{T} was estimated from a mean global myocardium TAC using the AIF in Eq. 1 and 2 (omitting the V_{RV} term). First, a one-parameter model was investigated, where the LV recovery coefficient β was estimated from the LV TAC $C_{\mathrm{PET,LV}}$ and AIF:

$$C_{\mathrm{PET,LV}}(t) = \beta C_{\mathrm{A}}(t) + (1 - \beta)C_{\mathrm{T}}(t). \tag{3}$$

An alternative two-parameter model did not constrain the sum of the coefficients to 1:

$$C_{\mathrm{PET,LV}}(t) = \beta_1 C_{\mathrm{A}}(t) + \beta_2 C_{\mathrm{T}}(t). \tag{4}$$

The sum $\beta 1 + \beta 2$ might be <1 if partial-volume mixing occurs with signal outside the heart (e.g., the lung).

To perform scale correction, the parameter β_{s} is estimated from:

Germino *et al. EJNMMI Research* (2016) 6:68

Page 4 of 12

$$C_{\text{PET,LV}}(t) = \beta_S C_A(t). \tag{5}$$

This correction was used by [5], with tracer-independent $\beta_s \approx 0.90$ estimated from canine ^{82}Rb and ^{13}N-ammonia PET and well counter measurements of arterial samples.

An alternative scale correction β_{AUC} was estimated as the ratio of the IDIF AUC to the AIF AUC:

$$\int_0^T C_{\text{PET,LV}}(t)\mathrm{dt} = \beta_{\text{AUC}} \int_0^T C_A(t)\mathrm{dt} \tag{6}$$

where T is the duration of the dynamic acquisition. While individually estimated β_{AUC} cannot outperform β_s in terms of weighted sum-of-squared residuals (WSS) (β_s minimizes WSS by design), a population-based β_{AUC} might give better kinetic parameter concordance.

Parameters for the one-parameter PVC, two-parameter PVC, and scaling models (Eq. 3, 4, and 5, respectively) were estimated via WLS for each acquisition. Model fits were compared by F tests. The ^{82}Rb K_1 estimates and ^{15}O-water k_2 estimates from AIFs were compared to those from β_{AUC} scale-corrected IDIFs by linear Deming regression, which models error in both variables, and by the Lin concordance coefficient [24], which provides a measure of absolute agreement between two estimates.

MBF estimation

Using myocardial VOIs (Fig. 1a), MBF was estimated from the mean myocardial ^{15}O-water k_2 values, corrected with a partition coefficient of $p = 0.91$ mL/g (MBF $= k_2 p$) [25]. Finally, the parameters a and b of the generalized Renkin-Crone model [5, 7, 8]

$$K_1 = \text{MBF} \cdot (1 - a e^{-b/\text{MBF}}) \tag{7}$$

were estimated from the mean myocardial ^{82}Rb K_1 values and ^{15}O-water MBF. In this model, b reflects the basal permeability-surface area (PS) product and a accounts for MBF-dependent PS changes. Fits used weighted orthogonal distance regression [26] to account for errors in both variables, with weights set to the reciprocals of the variance of voxel values in the myocardium VOIs. There were two datapoints per subject (rest and stress). Renkin-Crone parameters were independently estimated from mean kinetic parameters using (1) uncorrected IDIFs, (2) scale-corrected IDIFs, and (3) AIFs. Analyses were also performed without the V_{RV} term and separately for the lateral and septal walls.

Results
Hemodynamics
Figure 2 compares rate-pressure products (RPPs) for each pair of ^{82}Rb and ^{15}O-water scans. Mean (±standard deviation) absolute percent difference between ^{82}Rb and ^{15}O-water RPP was 12 ± 9 % at rest and 11 ± 9 % under pharmacological stress. Two subjects had RPPs with greater than 20 % difference between ^{82}Rb and ^{15}O-water scans at rest, and two subjects had RPPs with greater than 20 % difference between ^{82}Rb and ^{15}O-water scans under pharmacological stress. No significant group differences between ^{82}Rb and ^{15}O-water RPPs were found for rest ($p = 0.40$) or stress ($p = 0.44$).

IDIF validation
Table 1 gives means and standard deviations of the percent differences (across seven subjects) in peak activity, tail activity, and AUC of uncorrected IDIFs with respect to AIFs. The peaks of the ^{82}Rb IDIFs were underestimated by 13 and 19 % (rest, stress) compared to the AIFs, with smaller bias in AUC. An ideal IDIF might be expected to have a higher peak value, since no correction for internal-body dispersion was applied to the AIFs. Mean percent differences for all ^{15}O-water metrics were within ±10 %. These results suggest that IDIF correction could be beneficial for ^{82}Rb kinetic modeling, due to poorer resolution from larger positron range and higher myocardium-to-blood-pool contrast.
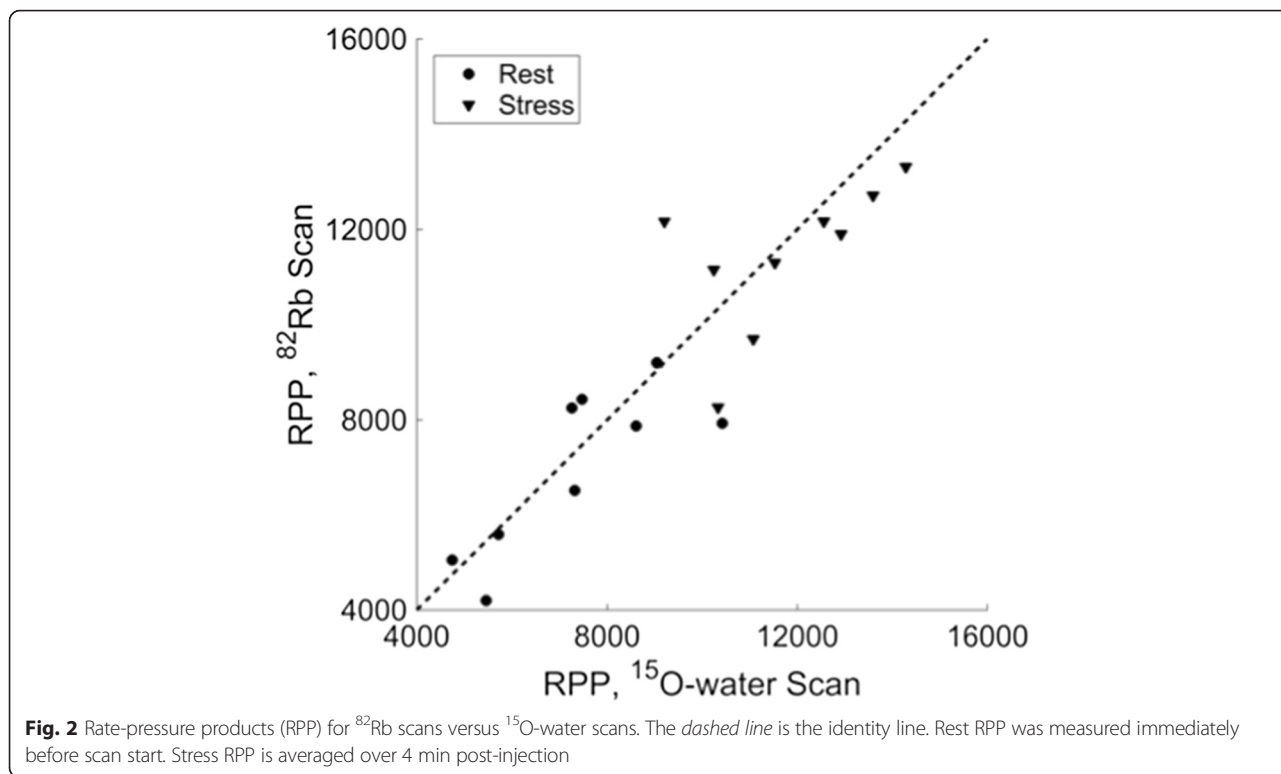
The mean and standard deviation of the parameter β from the one-parameter PVC model (Eq. 3) was 0.87 ± 0.09 (0.86 ± 0.12) for ^{82}Rb (^{15}O-water), which are similar to the 0.85 assumed by [13]. However, the tails of ^{82}Rb IDIFs corrected by this method were consistently underestimated (-54 ± 29 %) compared to the AIFs; neither the two-parameter PVC model (Eq. 4) nor scaling model (Eq. 5) demonstrated this deficiency (Fig. 3a). For ^{15}O-water IDIFs, there was no apparent qualitative difference among correction methods (Fig. 3b).

Using the two-parameter PVC method, the mean and standard deviation of $\beta_1 + \beta_2$ (Eq. 4) were 0.85 ± 0.10 (0.98 ± 0.10) for ^{82}Rb (^{15}O-water). This indicates that while a partial-volume mixture model of arterial blood and myocardium tissue may be sufficient for water, rubidium could require a different model of recovery-diminishing effects.

The mean and standard deviation of the scaling parameter β_s (Eq. 5) was 0.83 ± 0.09 (0.94 ± 0.10) for ^{82}Rb (^{15}O-water). The scaling parameter β_{AUC} (Eq. 6) was 0.92 ± 0.12 (0.97 ± 0.10) for ^{82}Rb (^{15}O-water). Additional file 1: Table S1 gives mean estimated correction parameters by tracer and condition.

Additional file 1: Figure S3 gives results of F-tests comparing the two-parameter PVC model to either the one-parameter PVC or scaling model (Eq. 5) for each acquisition. For 11 of 14 ^{82}Rb scans, the two-parameter PVC model outperformed the one-parameter PVC model. For only four ^{82}Rb scans, the two-parameter model outperformed scaling with β_s. For most ^{15}O-water

Germino *et al. EJNMMI Research* (2016) 6:68

Page 5 of 12

Fig. 2 Rate-pressure products (RPP) for ^{82}Rb scans versus ^{15}O-water scans. The *dashed line* is the identity line. Rest RPP was measured immediately before scan start. Stress RPP is averaged over 4 min post-injection

acquisitions, the two-parameter model was not superior to either one-parameter model (Eqs. 3 and 5).

The AUC scale correction (Eq. 6) cannot be compared to scaling with β_s by F-test, since the WSS of the AUC scale correction will always be at least that of the β_s correction. With the β_s correction, the difference in IDIF peak compared to AIF peak was 1 ± 17 % (3 ± 17 %) for ^{82}Rb (^{15}O-water); the difference in AUC becomes 10 ± 15 % (3 ± 10 %) for ^{82}Rb (^{15}O-water). With the β_{AUC} correction, the difference in peaks becomes -9 ± 16 % (0 ± 17 %) for ^{82}Rb (^{15}O-water); the difference in AUC becomes 0 ± 13 % (0 ± 10 %) for ^{82}Rb (^{15}O-water). Though β_s correction provides better peak agreement, β_{AUC} correction improves the peak agreement while also improving AUC agreement.

Based on these results, AUC-based scaling correction was adopted. All IDIFs were corrected by multiplication

with the reciprocal of the average β_{AUC} per tracer (1.09 for ^{82}Rb, 1.03 for ^{15}O-water). Eleven of 14 ^{82}Rb and 10 of 14 ^{15}O-water IDIFs had better agreement (lower WSS) with the AIF after scaling, with an average decrease in WSS of 18 ± 23 and 3 ± 16 %, respectively.

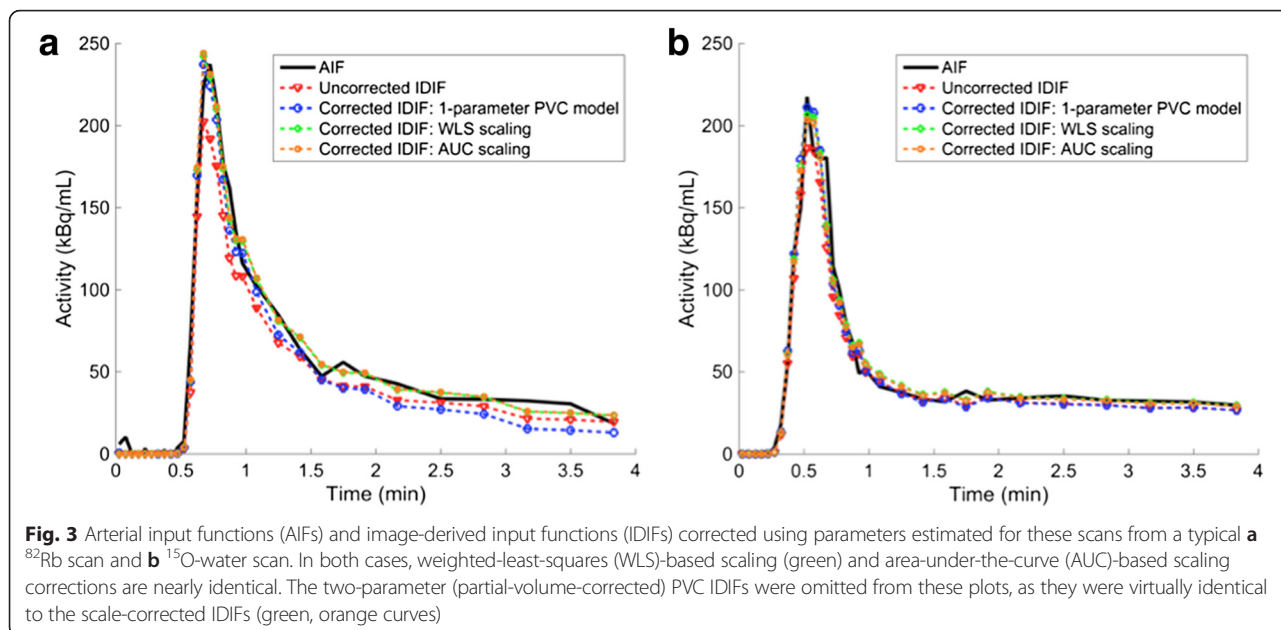### Parametric images

Example parametric images for one subject from the three-parameter fit are shown in Fig. 4, using each of: AIF, scaled IDIF, and uncorrected IDIF (Additional file 1: Figure S4 shows parametric images with and without the V_{RV} term). K_1 is an estimate of MBF for ^{15}O-water and nonlinearly related to MBF for ^{82}Rb due to incomplete extraction, so myocardial K_1 (Fig. 4a) is lower for ^{82}Rb than ^{15}O-water (note different display scales). Naturally, stress values exceed rest values for both tracers. Because we studied healthy subjects, K_1 is relatively uniform in

Table 1 Comparison of uncorrected IDIFs to AIFs

		AUC	Peak	Tail
		% difference mean ± SD	% difference mean ± SD	% difference mean ± SD
^{82}Rb	Rest	−11 ± 12	−13 ± 9.2	−7.1 ± 18
	Stress	−6.0 ± 13	−19 ± 18	2.6 ± 23
^{15}O-water	Rest	−5.1 ± 10	−8.4 ± 14	−5.4 ± 9.0
	Stress	−1.2 ± 9.9	2.4 ± 18	−3.5 ± 7.8

SD standard deviation, *AIF* arterial sample-based input function, *IDIF* image-derived input function, *AUC* area under curve, *% difference* 100 × (IDIF − AIF)/AIF

Germino et al. EJNMMI Research (2016) 6:68

Page 6 of 12

Fig. 3 Arterial input functions (AIFs) and image-derived input functions (IDIFs) corrected using parameters estimated for these scans from a typical **a** ^{82}Rb scan and **b** ^{15}O-water scan. In both cases, weighted-least-squares (WLS)-based scaling (green) and area-under-the-curve (AUC)-based scaling corrections are nearly identical. The two-parameter (partial-volume-corrected) PVC IDIFs were omitted from these plots, as they were virtually identical to the scale-corrected IDIFs (green, orange curves)

the myocardium. The LV cavity is more blurred in the K_1 images at stress than at rest for both tracers, presumably due to greater motion during stress. K_1 images are noisiest for ^{15}O-water stress, where higher k_2 results in greater correlation between K_1 and V_A, posing a more difficult estimation problem. The noisy ^{82}Rb k_2 images (Fig. 4b) show poor delineation of the myocardium due to minimal tracer washout, as rubidium is trapped by viable myocardial tissue. In contrast, ^{15}O-water freely diffuses in and out of tissue, so k_2 is proportional to MBF, and the k_2 images mirror the K_1 images. In the blood pool, k_2 values are very noisy since k_2 has minimal effect on model fits with $K_1 \approx 0$. Since the V_{RV} term was not included here, both the RV and LV blood pools are distinctly visible in the V_A images (Fig. 4c). V_A is overestimated from images using the uncorrected IDIF as compared to the AIF or scaled IDIF. The ^{15}O-water V_A images are slightly sharper than the ^{82}Rb V_A images, particularly near the septum, which may be explained by the poorer resolution of ^{82}Rb.

For this subject, the ^{82}Rb K_1 images from corrected IDIFs showed qualitatively better agreement with those from AIFs than those using uncorrected IDIFs (Fig. 4a). Because corrected IDIFs were generated using a population-based correction factor, not all scans had comparable improvement in agreement between corrected IDIF- and AIF-based images. The IDIF correction factor was closer to unity for ^{15}O-water than ^{82}Rb, so ^{15}O-water K_1 images were less affected by IDIF correction. The IDIF correction had virtually no impact on k_2 parametric images (Fig. 4b), as K_1 and V_A compensate changes in input function scale.

Table 2 lists mean myocardial parameter estimates across subjects (using subject-specific regions) for the uncorrected IDIFs, scaled IDIFs, and AIFs (three-parameter fit; see Additional file 1: Table S2 for four-parameter results). Standard deviations as a percent of the mean are similar between tracers for K_1. The V_A estimates, which account for both fractional blood volume and partial-volume effects, are lower for ^{15}O-water than ^{82}Rb, presumably due to the better resolution of ^{15}O. The K_1 data agreed better between the scaled IDIF and AIF estimates than between the uncorrected IDIF and AIF estimates; k_2 estimates were similar for all IFs.

This study's mean ^{82}Rb rest and stress K_1 and k_2 estimates using scaled IDIFs were comparable to those reported by [11]. The V_A estimates were approximately 20 % lower than those in [11], likely attributable to IDIF correction and the improved resolution of this study's images.

Figure 5a, b shows the good concordance between corrected IDIF- and AIF-based ^{82}Rb K_1 and ^{15}O-water k_2 mean myocardial estimates, respectively. Regression slopes (±standard error) for both ^{82}Rb K_1 and ^{15}O-water k_2 were close to 1.0 (1.06 ± 0.23 and 1.05 ± 0.36, respectively), and both intercepts were nearly 0 (0.025 ± 0.12 and -0.027 ± 0.51, respectively). The concordance correlation coefficient was 0.84 for both ^{82}Rb K_1 and ^{15}O-water k_2. Datapoints with poorer concordance may indicate subject motion, particularly during stress acquisitions, which affects the accuracy of IDIFs.

Extraction fraction parameter estimates
Figure 6 shows the Renkin-Crone model fits based on three-parameter kinetic model fits using scaled IDIFs;

Germino *et al. EJNMMI Research* (2016) 6:68

Page 7 of 12
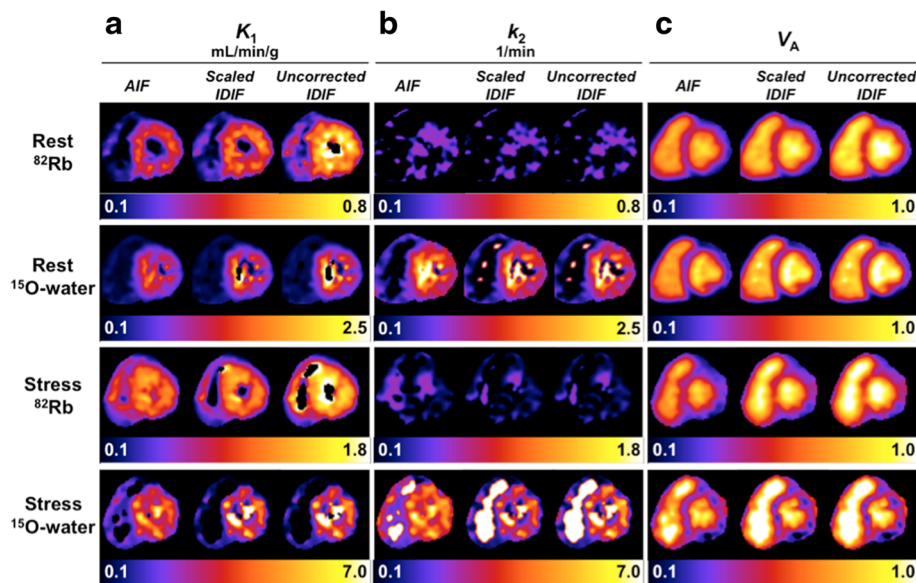
Fig. 4 Short-axis parametric images for one subject's ^{15}O-water and ^{82}Rb rest and stress scans, generated with different input functions. **a** K_1 parametric images, **b** k_2 parametric images, and **c** V_A parametric images. Background outside the heart has been omitted for display. *AIF* arterial sample-based input function, *IDIF* image-derived input function. Right ventricle spillover correction term (V_{RV}) not included

Table 3 gives corresponding parameter estimates. The V_{RV} term did not greatly impact Renkin-Crone fits estimated from global myocardial parameters, though omitting it resulted in greater differences between separate septal and lateral regional fits (Additional file 1: Figure S8). Figure 7 and Table 3 compare this study's extraction model parameter estimates (with and without IDIF correction) to several previously published fits. This study's *a* estimates are in reasonable agreement with that of the six comparison studies. Though the parameter *b* estimated using uncorrected IDIFs agrees with previous estimates, IDIF correction results in reduced *b*. The standard error of the
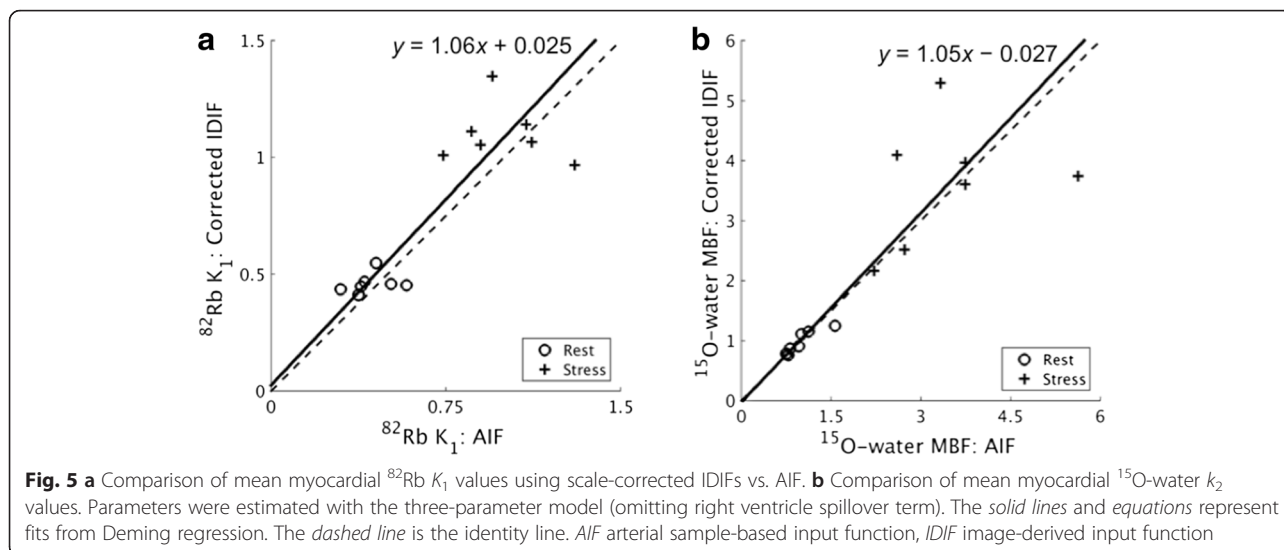
estimates of *a* and *b* of this study were similar to or lower than those previously published.

MBF estimated from ^{15}O-water k_2 (^{82}Rb K_1) was 0.96 ± 0.20 (0.91 ± 0.19) at rest and 3.73 ± 0.96 (3.59 ± 0.55) under pharmacological stress (Table 4). These flows are consistent with previously published measurements in healthy controls [27]. A Bland-Altman analysis shows no systematic bias between ^{82}Rb and ^{15}O-water flows ($p = 0.51$ for paired *t* test; Fig. 8). The reproducibility coefficient, defined as 1.96 times the standard deviation of the differences between the water and rubidium-based MBFs, normalized to the mean of

Table 2 Mean kinetic parameter estimates from three-parameter fit (without V_{RV})

			AIF	Scaled IDIF	Uncorrected IDIF
K_1 (mL/min/g) mean ± SD	Rest	^{82}Rb	0.43 ± 0.09	0.45 ± 0.05	0.53 ± 0.06
		$H_2^{15}O$	0.87 ± 0.21	0.86 ± 0.15	0.91 ± 0.16
	Stress	^{82}Rb	0.99 ± 0.19	1.11 ± 0.13	1.30 ± 0.17
		$H_2^{15}O$	3.43 ± 1.62	3.53 ± 0.85	3.68 ± 0.89
k_2 (1/min) mean ± SD	Rest	^{82}Rb	0.11 ± 0.05	0.13 ± 0.04	0.13 ± 0.04
		$H_2^{15}O$	1.10 ± 0.31	1.05 ± 0.22	1.05 ± 0.22
	Stress	^{82}Rb	0.21 ± 0.06	0.23 ± 0.08	0.23 ± 0.08
		$H_2^{15}O$	3.76 ± 1.24	4.10 ± 1.06	4.10 ± 1.06
V_A mean ± SD	Rest	^{82}Rb	0.32 ± 0.05	0.37 ± 0.04	0.40 ± 0.05
		$H_2^{15}O$	0.29 ± 0.08	0.33 ± 0.05	0.34 ± 0.06
	Stress	^{82}Rb	0.31 ± 0.06	0.40 ± 0.06	0.44 ± 0.06
		$H_2^{15}O$	0.27 ± 0.06	0.27 ± 0.06	0.28 ± 0.06

SD standard deviation, *AIF* arterial sample-based input function, *IDIF* image-derived input function

Fig. 5 a Comparison of mean myocardial ^{82}Rb K_1 values using scale-corrected IDIFs vs. AIF. **b** Comparison of mean myocardial ^{15}O-water k_2 values. Parameters were estimated with the three-parameter model (omitting right ventricle spillover term). The *solid lines* and *equations* represent fits from Deming regression. The *dashed line* is the identity line. *AIF* arterial sample-based input function, *IDIF* image-derived input function

each water-rubidium pair, was 39 %. While this study used ^{15}O-water MBF estimated from k_2, K_1-based flows were similar (Additional file 1: Figures S7 and S8).

Discussion

This study estimated Renkin-Crone extraction model parameters for rubidium using state-of-the-art ^{82}Rb and ^{15}O-water TOF PET images with PSF reconstruction. IDIF estimation was validated with continuously sampled arterial blood measurements (AIFs).

Armstrong et al. [16] provided a comparison of reconstructions with TOF and PSF to standard reconstructions; they reported an average increase in MBF of 10–14 % in advanced reconstructions compared to standard OSEM, which is consistent with improved recovery of signal in the myocardium. Because that study used only ^{82}Rb, extraction could not be estimated from the advanced reconstructions.

The PSF modeling used here was not isotope-specific. Because ^{15}O and ^{82}Rb have poorer resolution than ^{18}F, the PSF modeling will provide only partial resolution recovery. Though the employed reconstruction should provide better resolution than reconstruction without PSF modeling, there is further room for improvement.

Fig. 6 Renkin-Crone model fit of K_1 and myocardial blood flow from three-parameter kinetic model using scale-corrected image-derived input function. The *dashed lines* represent 95 % confidence interval of the regression line
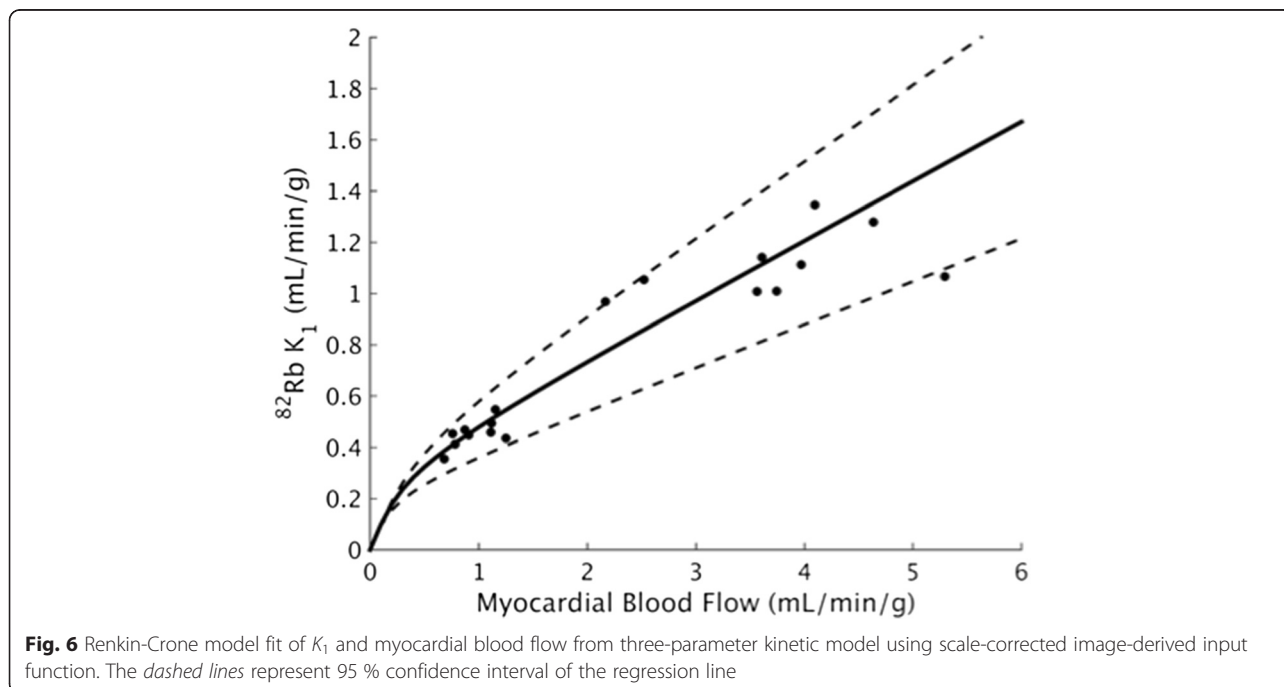
Table 3 Renkin-Crone parameter estimates from this and published studies

	Species	Flow measurement	Kinetic model	Input function correction	Renkin-Crone parameter estimates	
					$a \pm$ SE	$b \pm$ SE
This study	Human	^{15}O-water	1TCM	None	0.74 ± 0.03	0.51 ± 0.09
				Scaling	0.77 ± 0.03	0.39 ± 0.06
Yoshida 1996 [5]	Dog	^{13}N-ammonia	Retention	Scaling	0.85 ± 0.03	0.45 ± 0.08
Lortie 2007 [11]	Human	^{13}N-ammonia	1TCM	None	0.77 ± 0.05	0.63 ± 0.17
Lautamaki 2009 [10]	Dog	Microspheres	1TCM	None	0.89	0.68
Prior 2012 [12]	Human	^{15}O-water	1TCM	None	0.80 ± 0.04	0.59 ± 0.14
Katoh 2012 [13]	Human	^{15}O-water	1TCM	2-parameter partial-volume correction	0.86	0.54
Renaud 2013 [30]	Human	^{13}N-ammonia	Retention	None	0.92	0.74

IDIF image-derived input function, *SE* standard error

Resolution modeling in PET reconstruction can produce ringing artifacts that significantly impact quantification [28]. These effects are most often detectible in simulation and phantom studies with well-defined object borders. Here, because of the additional blurring incurred by uncompensated cardiac and respiratory motion and modest Gaussian filtering applied pre-modeling, Gibbs-like artifacts were not observed.

While PSF modeling and TOF can provide improved resolution, the primary benefit in this application is reduced noise in the parametric images. For representative maps of the standard error of ^{82}Rb K_1 and ^{15}O-water k_2, see Additional file 1: Figure S9.

In 3D PET with high injected activities, inaccurate corrections for detector deadtime can impact the accuracy of reconstructed activity in early frames. A previous patient study on the Biograph mCT suggests that doses of ^{82}Rb <1110 MBq can avoid significant detector saturation [29]. The doses used in the present study were on average ~60 % of this, and none exceeded it. Based on the peak singles rates, the average peak deadtime was 35 ± 8 % (32 ± 7 %) for ^{82}Rb (^{15}O-water).

PET image resolution is affected by positron range, detector resolution, smoothing in the reconstruction, and motion. Poor resolution affects quantification of myocardial activity and IDIFs. To minimize the impact of these effects on IDIFs, VOIs are typically small and central in the blood cavity where spill-in and spill-out are presumed insignificant. IDIF accuracy is important to kinetic modeling results; simulations show that a
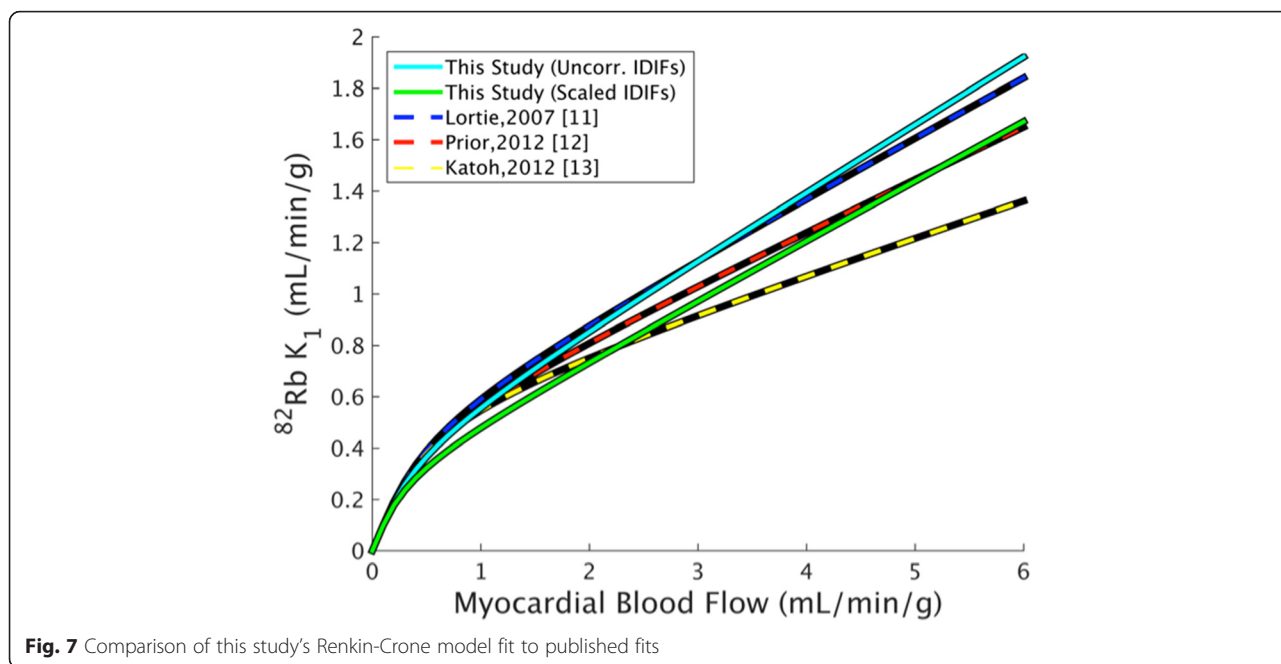
Fig. 7 Comparison of this study's Renkin-Crone model fit to published fits

Germino *et al. EJNMMI Research* (2016) 6:68

Page 10 of 12

Table 4 Extraction-corrected population estimates of myocardial blood flow, mean (±standard deviation)

		^{82}Rb MBF (mL/min/g)	^{15}O-water MBF (mL/min/g)
Uncorrected IDIF	Rest	0.92 ± 0.19	0.96 ± 0.20
	Stress	3.65 ± 0.64	3.73 ± 0.96
Scaled IDIF	Rest	0.91 ± 0.19	0.96 ± 0.20
	Stress	3.59 ± 0.55	3.73 ± 0.96

IDIF image-derived input function, *MBF* myocardial blood flow

10 % error in the IF peak can bias ^{82}Rb K_1 estimates by up to 25 % [18]. Thus, verification of IDIF accuracy is highly important.

IDIFs had lower correspondence with AIFs for rubidium than water, particularly in terms of peak activity. Unlike water, rubidium is retained in myocardial tissue, causing the tail of the blood pool TAC to fall below that of the myocardium TAC (water IDIFs will have matched activity in the tails of the LV cavity and myocardium TACs). When ^{82}Rb images are degraded by motion and resolution effects, expected consequences for IDIFs are reduced peak activity (spill-out from LV cavity) and increased tail activity (spill-in from myocardium). Though prior publications' images [11, 12] were likely of poorer resolution than this study's, their IDIFs were uncorrected. In the current study, we primarily observed reduced peak activity in ^{82}Rb IDIFs, with differences in tail activity inconsistent with a strict model of geometric PVC (Eq. 3). In Katoh et al. [13], LV TACs were corrected using a PVC model; that model overcorrected the tails of our ^{82}Rb IDIFs. A mismatch between ^{82}Rb IDIFs and AIFs was better described using a

two-parameter model (Eq. 4), which provides for signal mixing with background regions. The simpler scale factor correction (Eq. 5), which recovers activity from an unspecified combination of resolution degradation effects, gave comparable results. For half the ^{82}Rb acquisitions, the AUC-based scale factor β_{AUC} (Eq. 6) was approximately equal to the scan-specific β_s (Eq. 5). For the rest, β_{AUC} was markedly higher than β_s; in these cases, the IDIF more greatly underestimated the AIF peak, with lower error in the tail. When β_s is used to correct these cases, though the average peak error is reduced to ~0, the average AUC is overestimated, because tail activity is overestimated.

We chose scaling IDIFs based on AUC matching as more appropriate than WLS-based scaling. For ^{15}O-water, the differences between the two methods were small. ^{82}Rb, however, is more sensitive to the input function AUC, as its uptake is approximately irreversible. For such tracers, tissue activity is directly proportional to the input function AUC, so errors in the AUC propagate into the parameter estimates.

Given our AIF measurements and anticipating that population-based IDIF correction is most practical for scans without arterial sampling, we used mean tracer-dependent scale factors to correct IDIFs. However, the optimal correction factor is scan-dependent, conditional on variations in VOI size and placement, heart size, breathing pattern, and subject motion. Further investigation is required to assess generalizability to other scanners and reconstruction algorithms. Using AIFs for modeling does not guarantee accurate parameter estimates, as error
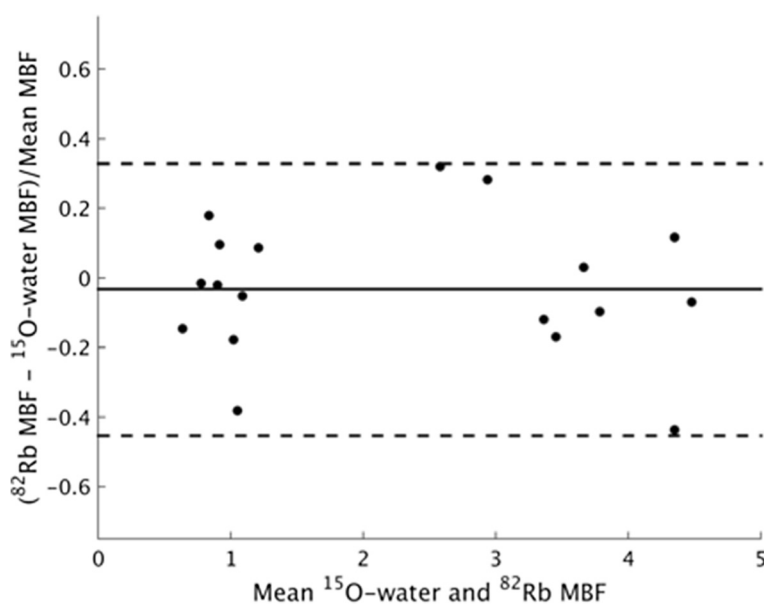
Fig. 8 Bland-Altman plot comparing ^{15}O-water myocardial blood flow (MBF) to ^{82}Rb MBF, using scaled image-derived input functions. Mean percent difference is −3.2 %. The *dashed lines* show 95 % confidence intervals

Germino *et al. EJNMMI Research* (2016) 6:68

Page 11 of 12

in myocardial TACs not addressed by the partial-volume fractions V_A and V_{RV} (Eq. 2) could induce bias. Body and respiratory motion are likely principal sources of error. One limitation this study shares with previous publications is that no motion compensation was incorporated.

The Renkin-Crone model fits obtained in this study are similar to previously published fits, though our b estimate is lower, primarily a reflection of lower ^{82}Rb K_1 estimates in this study compared to others, from the IDIF correction that was applied. With uncorrected IDIFs, extraction parameters obtained in this study closely match those previously published by Lortie [11]. Because scaling correction impacts ^{82}Rb K_1 but not ^{15}O-water k_2, scaled IDIFs resulted in a decrease in the b parameter of the Renkin-Crone model. For most previous studies, there was no gold standard measurement of the input function, and therefore, no basis for IDIF correction. Katoh et al. [13] used partial-volume corrected IDIFs, which explains the better agreement between their extraction model and that from corrected IDIFs in this study, compared to the Lortie model. The a parameter of the Renkin-Crone model is less sensitive to IDIF correction and reported values vary less across the literature.

Some differences in Renkin-Crone fits can also be explained by the flow estimation method. For instance, [11] used ^{13}N-ammonia to measure MBF, which has a lower extraction fraction than ^{15}O-water and will hence underestimate MBF. Using unweighted ODR to fit the data instead of weighted ODR resulted in higher parameter estimates (Additional file 1: Figure S10). Average MBFs were similar regardless of IDIF correction because water-based flows were unaffected by IDIF scaling and extraction parameters were estimated separately for each case. Therefore, accurate flows can be determined for ^{82}Rb with or without IDIF correction, if extraction parameters have been estimated from data processed similarly. This suggests that modeling choices could have greater impact on extraction fraction estimates than TOF and PSF modeling, though TOF/PSF-based kinetic parameters have lower standard error.

Conclusions

We have presented parameter estimates for the generalized Renkin-Crone model of extraction for ^{82}Rb PET using human ^{82}Rb and ^{15}O-water PET from high-resolution images from a state-of-the-art TOF-capable scanner with PSF reconstruction. The image-derived input functions were validated against direct arterial measurements, and a scale correction improved the accuracy of IDIFs. With this IDIF correction, MBF should be estimated from ^{82}Rb K_1 using the Renkin-Crone parameters reported here. These results provide a state-of-the-art methodology for MBF measurement with ^{82}Rb PET, though further validation will be necessary in patients with coronary artery disease with infarcts and ischemia.

Additional file

Additional file 1: Figures S1–S10 and Tables S1–S2. (PDF 2.93 mb)

Author details
^{1}Biomedical Engineering, Yale University, New Haven, CT, USA. ^{2}PET Center, Diagnostic Radiology, School of Medicine, Yale University, New Haven, CT, USA. ^{3}Yale Cardiovascular Research Center, Section of Cardiovascular Medicine, Department of Internal Medicine, Yale University, New Haven, CT, USA. ^{4}PET Center, Yale School of Medicine, PO Box 208048, New Haven, CT 06520-8048, USA.

References

1. Grover-McKay M, Ratib O, Schwaiger M, Wohlgelernter D, Araujo L, Nienaber C, et al. Detection of coronary artery disease with positron emission tomography and rubidium 82. Am Heart J. 1992;123:646–52.
2. Parkash R, Ruddy T, Kitsikis A, Hart R, Beauschene L, Williams K, et al. Potential utility of rubidium 82 PET quantification in patients with 3-vessel coronary artery disease. J Nucl Cardiol. 2004;11:440–9.
3. Sampson UK, Dorbala S, Limaye A, Kwong R, Di Carli MF. Diagnostic accuracy of rubidium-82 myocardial perfusion imaging with hybrid positron emission tomography/computed tomography in the detection of coronary artery disease. J Am Coll of Cardiol. 2007;49:1052–8.
4. Ziadi MC, Williams K, Guo A, Renaud JM, Chow BJ, Klein R, et al. Does quantification of myocardial flow reserve using rubidium-82 positron

Germino *et al. EJNMMI Research* (2016) 6:68

Page 12 of 12

emission tomography facilitate detection of multivessel coronary artery disease? J Nucl Cardiol. 2012;19:670–80.

5. Yoshida K, Mullani N, Gould KL. Coronary flow and flow reserve by PET simplified for clinical applications using rubidium-82 or nitrogen-13-ammonia. J Nucl Med. 1996;37:1701–12.

6. Mullani NA, Goldstein RA, Gould KL, Marani SK, Fisher DJ, O'Brien HA, et al. Myocardial perfusion with rubidium-82. I. Measurement of extraction fraction and flow with external detectors. J Nucl Med. 1983;24:898–906.

7. Renkin EM. Transport of potassium-42 from blood to tissue in isolated mammalian skeletal muscles. Am J Physiol. 1959;197:297.

8. Crone C. The permeability of capillaries in various organs as determined by use of the 'indicator diffusion' method. Acta Physiol Scand. 1963;58:292–305.

9. Moody J, Murthy V, Lee B, Corbett J, Ficaro E. Variance estimation for myocardial blood flow by dynamic PET. IEEE Trans Med Imag. 2015;34:2343–2353.

10. Lautamäki R, George RT, Kitagawa K, Higuchi T, Merrill J, Voicu C, et al. Rubidium-82 PET-CT for quantitative assessment of myocardial blood flow: validation in a canine model of coronary artery stenosis. Eur J Nucl Med Mol Imaging. 2009;36:576–86.

11. Lortie M, Beanlands RS, Yoshinaga K, Klein R, DaSilva JN. Quantification of myocardial blood flow with 82Rb dynamic PET imaging. Eur J Nucl Med Mol Imaging. 2007;34:1765–74.

12. Prior JO, Allenbach G, Valenta I, Kosinski M, Burger C, Verdun FR, et al. Quantification of myocardial blood flow with 82Rb positron emission tomography: clinical validation with 15O-water. Eur J Nucl Med Mol Imaging. 2012;39:1037–47.

13. Katoh C, Yoshinaga K, Klein R, Kasai K, Tomiyama Y, Manabe O, et al. Quantification of regional myocardial blood flow estimation with three-dimensional dynamic rubidium-82 PET and modified spillover correction model. J Nucl Cardiol. 2012;19:763–74.

14. Tipnis S, Hu Z, Gagnon D, O'Donnell J. Time-of-flight PET for Rb-82 cardiac perfusion imaging. J Nucl Med. 2008;49:74.

15. DiFilippo F, Brunken R. Benefit of time-of-flight reconstruction for cardiac PET of obese patients [Abstract]. J Nucl Med Soc Nuclear Med. 2013;54:405.

16. Armstrong IS, Tonge CM, Arumugam P. Impact of point spread function modeling and time-of-flight on myocardial blood flow and myocardial flow reserve measurements for rubidium-82 cardiac PET. J Nucl Cardiol. 2014;21:467–74.

17. Presotto L, Gianolli L, Gilardi M, Bettinardi V. Evaluation of image reconstruction algorithms encompassing time-of-flight and point spread function modelling for quantitative cardiac PET: phantom studies. J Nucl Cardiol. 2015;22:351–63.

18. Meyer C, Peligrad D-N, Weibrecht M. Assessment of input function distortions on kinetic model parameters in simulated dynamic 82 Rb PET perfusion studies. Nucl Instrum Meth A. 2007;571:199–202.

19. Weinberg I, Huang S, Hoffman E, Araujo L, Nienaber C, McKay MG, et al. Validation of PET-acquired input functions for cardiac studies. J Nucl Med. 1988;29:241–7.

20. Murthy VL, Lee BC, Sitek A, Naya M, Moody J, Polavarapu V, et al. Comparison and prognostic validation of multiple methods of quantification of myocardial blood flow with 82Rb PET. J Nucl Med. 2014;55:1952–8.

21. Coxson PG, Huesman RH, Borland L. Consequences of using a simplified kinetic model for dynamic PET data. J Nucl Med. 1997;38:660.

22. Bergmann S, Fox K, Rand A, McElvany K, Welch M, Markham J, et al. Quantification of regional myocardial blood flow in vivo with H215O. Circulation. 1984;70:724–33.

23. Lodge MA, Carson RE, Carrasquillo JA, Whatley M, Libutti SK, Bacharach SL. Parametric images of blood flow in oncology PET studies using [15O] water. J Nucl Med. 2000;41:1784–92.

24. Lawrence I, Lin K. A concordance correlation coefficient to evaluate reproducibility. Biometrics. 1989;45:255–68.

25. Iida H, Kanno I, Takahashi A, Miura S, Murakami M-t, Takahashi K, et al. Measurement of absolute myocardial blood flow with H215O and dynamic positron-emission tomography. Strategy for quantification in relation to the partial-volume effect. Circulation. 1988;78:104–15.

26. Boggs PT, Donaldson JR, Schnabel RB. Algorithm 676: ODRPACK: software for weighted orthogonal distance regression. ACM Trans Math Softw. 1989; 15:348–64.

27. Sdringola S, Johnson NP, Kirkeeide RL, Cid E, Gould KL. Impact of unexpected factors on quantitative myocardial perfusion and coronary flow reserve in young, asymptomatic volunteers. JACC Cardiovasc Imaging. 2011; 4:402–12.

28. Tong S, Alessio AM, Thielemans K, Stearns C, Ross S, Kinahan PE. Properties and mitigation of edge artifacts in PSF-based PET reconstruction. Nucl Sci IEEE Trans. 2011;58:2264–75.

29. Tout D, Tonge CM, Muthu S, Arumugam P. Assessment of a protocol for routine simultaneous myocardial blood flow measurement and standard myocardial perfusion imaging with rubidium-82 on a high count rate positron emission tomography system. Nucl Med Commun. 2012;33:1202–11.

30. Renaud JM, DaSilva JN, Beanlands RS. Characterizing the normal range of myocardial blood flow with 82rubidium and 13 N-ammonia PET imaging. J Nucl Cardiol. 2013;20:578–91.